ADVANCED FUNCTIONAL MATERIALS
www.afm-journal.de

Gradient Porous Elastic Hydrogels with Shape-Memory Property and Anisotropic Responses for Programmable Locomotion

*Rongcong Luo, Jin Wu, Ngoc-Duy Dinh, and Chia-Hung Chen**

Programmable locomotion of responsive hydrogels has gained increasing attention for potential applications in soft robotics, microfluidic components, actuators, and artificial muscle. Modulation of hydrogel pore structures is essential for tailoring their mechanical strength, response speeds, and motion behaviors. Conventional methods forming hydrogels with homogeneous or stepwise-distributed pore structures are limited by the required compromise to simultaneously optimize these aspects. Here, a heterobifunctional crosslinker enabled hydrothermal process is introduced to synthesize responsive hydrogels with well-defined gradient pore construction. According to gradient porosity controls, the hydrogels simultaneously exhibit rapid responses to external stimuli, high elasticity/compressibility, and programmable locomotion capability. By incorporating polypyrrole nanoparticles as photothermal transducers, photo/thermal responsive composite hydrogels are formed to enable programmable control of locomotion such as bending, curving, twisting, and octopus-like swimming under near-infrared laser stimulation. The tunable pore structures, mechanical properties, and locomotion of this new class of materials make these gradient porous hydrogels potentially suitable for a variety of applications.

1. Introduction

Stimuli-responsive hydrogels can convert exogenous stimuli into user-defined functions, such as conversion of light/heat into mechanical works and conversion of biochemical signals into size/shape changes.[1–3] Consequently, they are playing an increasingly important role in various applications, such as artificial muscles,[4] microfluidic valves,[5] actuators,[6] soft robotics,[7] drug carrier,[8] and microlenses.[9] Rapid response, robust mechanical strength, and programmable locomotion capability are essential to the applications. However, there are compromises that must be made to simultaneously optimize all these aspects. Conventional hydrogels exhibit slow macroscale response with a magnitude of minutes to hours.[10–13] Meanwhile, they are typically mechanically weak or brittle,[14,15] resulting in unstable performance after cycles of stimulation. In addition, most of these hydrogels possess isotropic porous structures, showing size changes evenly, making desirable locomotion (e.g., bending, twisting, and folding) difficult to achieve.[16,17]

Modulation of pores size and their distributions is essential for manipulating hydrogels properties. Several strategies including gas foaming,[18] fiber bonding,[19] and porogen leaching[20] were developed to fabricate homogeneous macropore sized hydrogels for rapid responses. However, the orientation responses of such materials were limited, causing difficulties in anisotropic locomotion. Moreover, mechanical strength of these hydrogels was relatively weak due to the fragile macrosized pore structures. On the other hand, electrophoresis-assisted porogen leaching and hydrogel layering methods[21–24] have been developed to produce responsive hydrogels with stepwise-distributed pore structures to enable their anisotropic responsive capabilities. However, these hydrogels have some adverse properties including less pore interconnectivity, decelerated mass transport, and being prone to delamination, causing their slow response to stimuli and poor mechanical properties. To date, synthesis of hydrogels with simultaneously rapid thermal response kinetics, robust mechanical strength, and desirable anisotropic locomotion remains an unsolved challenge.

In this study, we presented a heterobifunctional crosslinker enabled hydrothermal process, forming hydrogels with gradient porous structure to address these issues. The hydrothermal synthesis is performed in closed systems of relatively high temperatures and pressures, in which only water is used as the reactive medium. At elevated temperatures, hydrothermal process can prompt a variety of chemical reactions such as vinyl polymerizations and intermolecular dehydration.[25–27] *N*-isopropylacrylamide (NIPAM), a well-known thermo-responsive material bearing two highly reactive double bonds,[28,29] was used as monomer. 4-hydroxybutyl acrylate (4HBA), an acrylic ester possessing a reactive double bond and a less reactive hydroxyl group at either end of the molecule, was innovatively applied

Dr. R. Luo, Dr. N.-D. Dinh, Dr. C.-H. Chen
Department of Biomedical Engineering
National University of Singapore
Singapore 117575, Singapore
E-mail: biecch@nus.edu.sg
Dr. J. Wu
School of Materials Science and Engineering
Nanyang Technological University
50 Nanyang Avenue, Singapore 639798, Singapore

DOI: 10.1002/adfm.201503434

as a heterobifunctional crosslinker. NIPAM was first polymerized with 4HBA via hydrothermally induced free radical vinyl polymerization, forming NIPAM polymer chains with pendant hydroxyl groups (PNIPAM-OH). The PNIPAM-OH precipitated and lead to a diminishing concentration gradient of PNIPAM-OH from top to bottom of the hydrothermal reactor. Along with the precipitation process, intermolecular dihydroxylation occurred via hydrothermally induced dehydration polymerization, forming gradient porous hydrogel. Response of the synthesized hydrogels is in instant manner (≈4 s), which is ≈20 times faster than previous stepwise porous hydrogels with similar dimensions.[21] Meanwhile, the hydrogels were highly elastic, which could withstand ≈95% strain without being fractured. Besides, polypyrrole (PPy) nanoparticles that act as photothermal nanotransducers could be loaded into the gradient porous hydrogels, forming a photo/thermal-responsive composite material. Based on the gradient porous size distributions, various programmable locomotion such as bending, curving, twisting, and octopus-like swimming could be induced through near-infrared (NIR) laser stimulation.

2. Results and Discussion

2.1. Hydrothermal Synthesis of Gradient Porous Hydrogels

Figure 1a schematically illustrates the reaction mechanism for hydrothermal formation of gradient porous hydrogel. NIPAM,

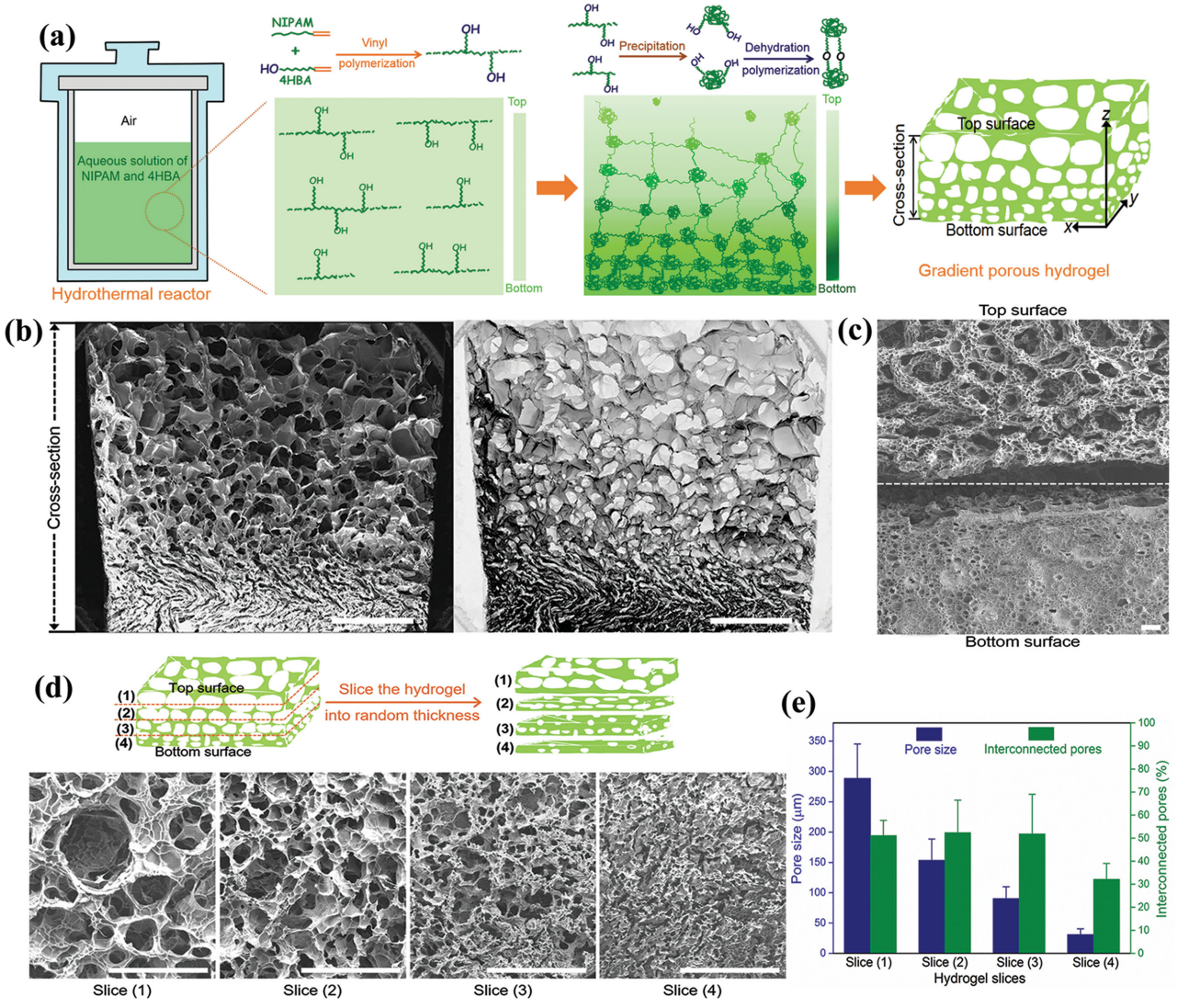

Figure 1. Hydrothermal synthesis of a gradient porous hydrogel. a) Scheme illustrating the reaction process of hydrothermally forming a gradient porous hydrogel. A pre-gel solution containing NIPAM and 4HBA in a hydrothermal reactor is heated. NIPAM is polymerized with 4HBA, forming NIPAM polymer chains with pendant hydroxyl groups. The polymer chains are precipitated and crosslinked to form a gradient porous hydrogel. b) SEM images showing a cross-section view of the hydrogel (left) and the corresponding inverted image (right), the scale bar is 1 mm. c) SEM observations on the top surface and bottom surface of the hydrogel, the scale bar is 100 μm. d) SEM investigations on the surface morphology of hydrogel slices with random thickness, showing a decreasing pore size from top to bottom surface of the hydrogel, the scale bar is 1 mm. e) Pore size and pore interconnectivity of each hydrogel slice.

4HBA, and APS were first dissolved in deionized water (DI H_2O) and filtered. The resulting solution was loaded into the hydrothermal reactor and heated at 180 °C for 4 h. After the reactor was cooled, hydrogel with gradient porous structures in the direction of the *z*-axis was obtained. SEM observations revealed reducing pores size along the cross section of the hydrogels (Figure 1b, left). The inverted SEM image clearly showed a continuous gradient pores ranging from nanoporous to macroporous features within an integrated hydrogel matrix (Figure 1b, right). Morphology of hydrogel top surface was distinctly different from that of the hydrogel bottom surface (Figure 1c). The bottom surface was dense and compact, whereas the top surface exhibited an interconnected macroporous structure, indicating the increasing porosity from bottom to top surface of the hydrogel. The gradient porous hydrogel was sliced into four pieces of hydrogel sheets with random thickness, and their pore size was investigated (Figure 1d). A gradual reduction in pore size from slice 1 (≈350 μm) to slice 4 (≈30 μm) was observed, indicating the continuously changing pore size features within the hydrogel. The pore interconnectivity of each hydrogel slice was further evaluated using a water-wicking technique.[30] Hydrogel slices 1, 2, and 3 exhibited similar pore interconnectivity of ≈55% relative to hydrogel slice 4, which exhibited pore interconnectivity of ≈30% (Figure 1e), ensuring fast and directional water diffusion within the hydrogel. Application of 4HBA as a novel heterobifunctional crosslinker played a critical role in forming the gradient porous structure. 4HBA possesses a reactive double bond and a less reactive hydroxyl group at either end of the molecule. Because of its heterogeneous reactivity, 4HBA enabled the polymerization of NIPAM monomers and gelation of NIPAM polymers to be implemented in a sequential (two-step) manner, thereby enabling formation of a gradient porous structure within the hydrogel. Briefly, during the initial hydrothermal stage, NIPAM monomers polymerized with 4HBA via hydrothermally induced free radical vinyl polymerization, generating NIPAM polymer chains with pendant hydroxyl groups (PNIPAM-OH). As the reaction progressed, PNIPAM-OH dissociates water and precipitates to the bottom of the hydrothermal reactor, leading to a diminishing concentration gradient of PNIPAM-OH from top to bottom. Along with the PNIPAM-OH precipitation process, the pendant hydroxyl groups were linked via hydrothermally induced dehydration polymerization, forming a gradient porous PNIPAM hydrogel (Sections S1 and S2, Supporting Information). For comparison to 4HBA, conventional homobifunctional crosslinker, *N*,*N*-methylenebisacrylamide (BIS) and the mixed crosslinker 4HBA/BIS were also, respectively, used to form PNIPAM hydrogels hydrothermally. Both BIS and 4HBA/BIS crosslinker systems exhibited faster hydrogelation kinetics compared to those of 4HBA (Sections S1 and S2, Supporting Information). However, the obtained hydrogels typically exhibited homogenously nanoporous features within the hydrogel matrix (Figures S10 and S12, Supporting Information).

2.2. Instant Directional Response of the Hydrogels

After being incubated at 40 °C water for 35 s, the original hydrogel (25 °C) with a diameter of 9 cm shrank upward and folded into a tube-like gel with dimensions of ≈2.25 cm × 3.5 cm, reaching ≈80% of the shape change (**Figure 2**a). The swelling/de-swelling processes of the hydrogel were highly reversible with the heating/cooling stimulations, where the gel exhibited no fatigue phenomena after ≈10 cycles of thermal stimulation (Figure 2c). To investigate the thermal response kinetics of the hydrogel, a hydrogel strip with defined dimensions of 40 mm × 4 mm × 2.5 mm was prepared and subjected to thermal stimulation. The thermal response time of the hydrogel strip was recorded according to the change of the end-to-end distance of the hydrogel strip (shown as the A to B distance in Figure 2b). The hydrogel had a thermal response time of 4 s, and 2 s were needed to reach 50% of the change of the end-to-end distance (Figure 2d), which was ≈20 times faster than previous porous hydrogel materials.[21] An eight point star-shaped hydrogel was sliced into four pieces of gel sheets with random thickness and subjected to thermal stimulation alternatively (Figure 2e). All four hydrogel slices exhibited similar thermal-responsive folding/unfolding motion, where the hydrogels in the folded state (40 °C) had a greater value of height than hydrogels in the unfolded state (25 °C) (Figure S14 and Video S1, Supporting Information). The results further demonstrated the merits of the continuously changing gradient porous features of the gels, where the gradually decreasing pore sizes synergistically gave the gels rapid thermal response and directional locomotion ability. The gradient pore structure can correspondingly generate a gradient swelling/de-swelling between top surface and bottom surface, driving the anisotropic motion of the hydrogels. Meanwhile, the continuously changing pore structure can facilitate water diffusion, leading to rapid responses. The gradient porous hydrogels are readily postmoldable. For example, hydrogel tubes/rings can be fabricated by thermally triggering a rectangular-shaped hydrogel strip (Figure 2b), finding applications in cell-sheet-based tissue engineering[31] and hands-free packaging.[32] Moreover, an eight-point star-shaped hydrogel can reversibly fold and unfold (Figure 2e), inspiring its application as soft microgrippers.[33]

2.3. Elasticity and Shape-Memory Properties of the Hydrogels

Along with the rapid response to external stimuli, the gradient porous hydrogels meanwhile were highly compressible with promising reversibility. They could be compressed and deformed up to 90% of their original size without being mechanically fractured. After the load was released, the deformed hydrogels immediately returned to their original shape in less than 1 s (**Figure 3**a). In contrast, hydrogels synthesized from BIS or BIS/4HBA crosslinkers exhibited inferior mechanical compressibility and reversibility. They were unable to return to their original size after being compressed under the same loading (Figure S15, Supporting Information). The process of compression and release was repeatedly applied to the same gradient porous hydrogel for three times, and the compressive stress–strain profiles were recorded (Figure 3b). After ≈95% compression, the hydrogel recovered its original shape after being rehydrated and recovered all of its properties, such as compressive modulus, radius, and height. The compressive modulus of the hydrogel was ≈7.3 ± 1.5 kPa, which

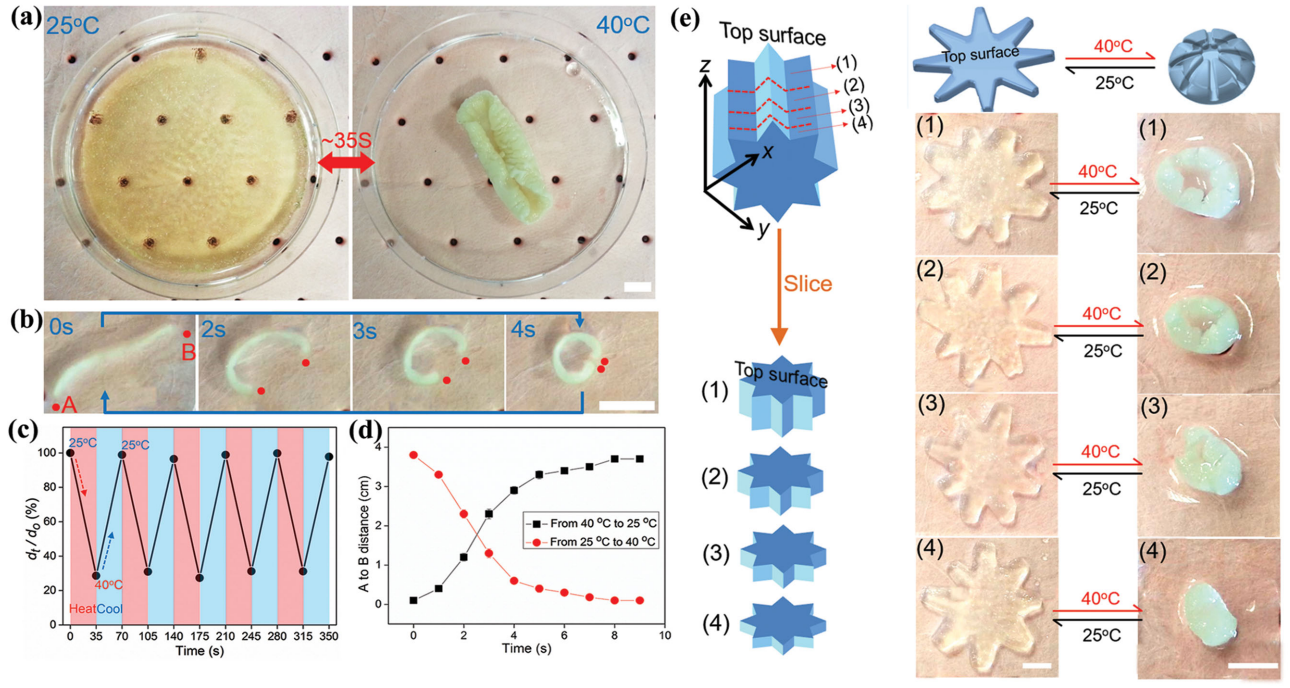

Figure 2. Thermally triggered response of hydrogels. a) Morphology of a gradient porous hydrogel at 25 and 40 °C, respectively, the scale bar is 1 cm. b) Morphology and thermal responsive time of a gradient porous hydrogel strip after being put into 40 °C H_2O, the scale bar is 1 cm. c) Reversible size changes to thermal stimulation and the thermal responsive time of the hydrogel shown in (a). d) Distance between two ends of the hydrogel strip after alternate heating/cooling and the corresponding thermal responsive time of the hydrogel strip shown in (b). e) An eight-point star shaped hydrogel is sliced into random thickness. These hydrogel slices show similar folding/unfolding motion after being triggered by thermal stimulus, the scale bar is 1 cm.

was in good agreement with the compressive modulus of previously reported elastic hydrogel.[30] Inspired by the reversible compressibility of the hydrogels, we tested their potential applications as shape-memory materials (Video S2, Supporting Information). As a demonstration, square-shaped, rectangle-shaped, triangle-shaped, and eight-point star-shaped hydrogels were tested for their shape-memory ability. First, the fully hydrated hydrogels were heated to 40 °C to expel the water and shrink the hydrogel. The shrunken hydrogels were then compressed and twisted into deformed shapes. The deformed hydrogels were subsequently placed into water to recover their original shape (Figure 3c). All of the shaped hydrogels were observed to maintain their permanent shapes, to be deformed and then to later be relaxed back to their original structure without residual deformation (Figure 3d). The shape recovery efficiency of these hydrogels was determined (Figure 3e). After being placed into water for ≈10 s, all the deformed hydrogels recovered greater than 98% of their original shapes, indicating the faithful shape-memory ability of these gradient porous elastic hydrogels. After being subjected to five cycles of the shape-memory processes, the gradient porous hydrogels retained compressive modulus similar to that of the original samples (Figure 3f), demonstrating the mechanical stability of the hydrogels. The gradient pore structure is not necessary in the shape-memory performance of the hydrogels. Shape-memory property of the hydrogel is resulted from the reversible collapse of the pores within the hydrogel materials. The processes of heating and compressing cause efflux of water from interconnected pores and collapse of the hydrogel structure. After removal of compressive stress, the stored elastic energy is released, and water is reabsorbed into the hydrogel, resulting in the recovery of the hydrogel's shape and structure.

2.4. PPy Loaded Hydrogels as Photomechanical Converter

By incorporating photothermal nanotransducer—PPy nanoparticles (Figure S16, Supporting Information), we transformed the gradient porous PNIPAM hydrogel, which inherently exhibits thermal responses, into a near-infrared (NIR) laser triggerable composite hydrogel (**Figure 4**a and Video S3, Supporting Information). The spongy features of the hydrogel can facilitate loading of PPy nanoparticles, where simple incubation of PPy nanoparticles aqueous solution with the hydrogels for 1 h can obtain an ≈70% of PPy nanoparticles loading efficiency. After the incubating and washing steps, the SEM images clearly indicated that the PPy nanoparticles with a monodisperse size of 90 nm were evenly distributed on the surface of the hydrogel pore walls (Figure 4a and Figure S19, Supporting Information). In contrast to the whole hydrogel curling that resulted from thermal stimulation, site-specific, length-controllable bending of the hydrogel occurred in response to NIR laser irradiation (980 nm, 2.5 W cm^{-2}), demonstrating the advantages of photostimulus over thermal stimulus (Figure S20, Supporting Information). Regardless of laser irradiation direction, top surface of the hydrogel kept bending toward the concave side (Figure 4b and Figure S21, Video S3, Supporting Information). The bending direction of the hydrogels can be conveniently

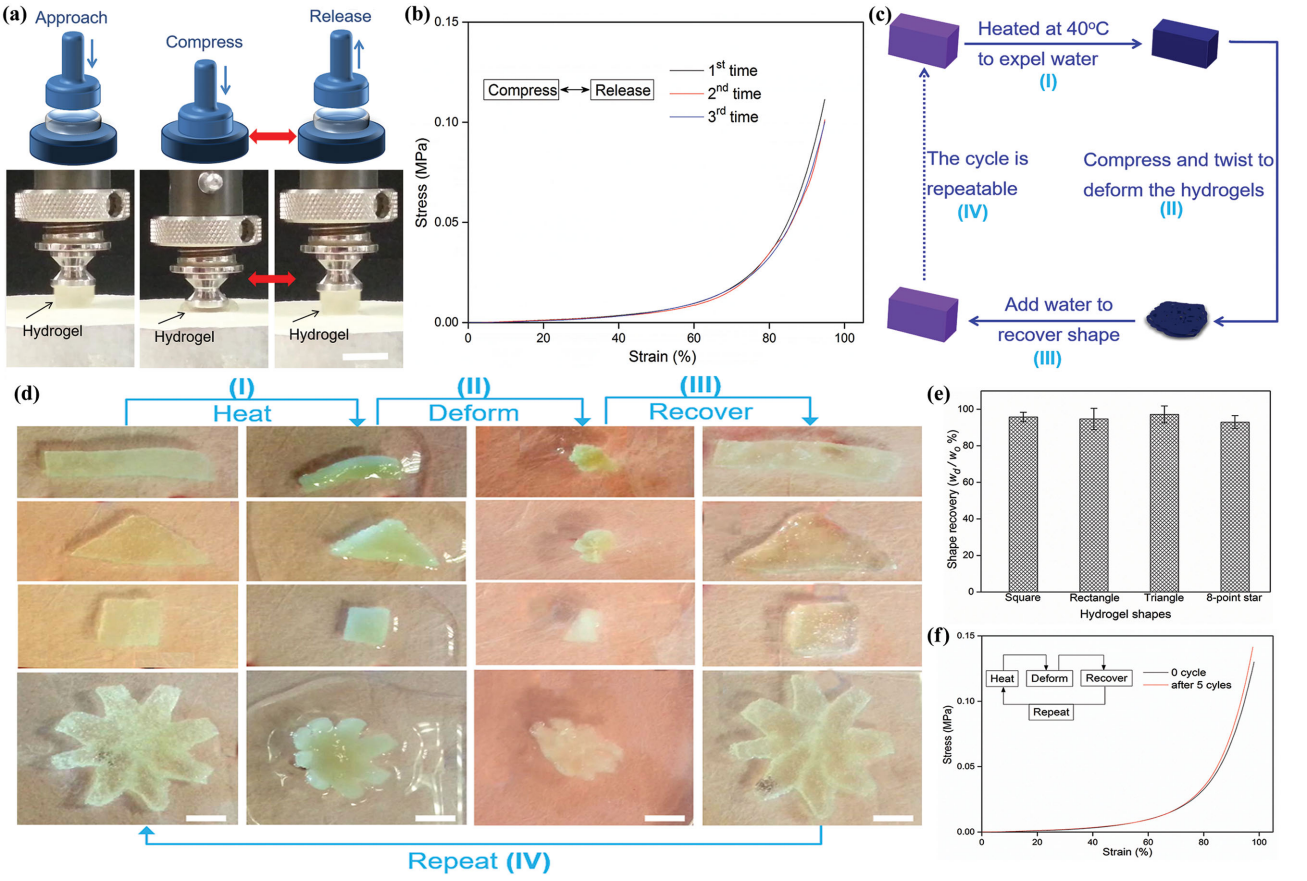

Figure 3. Elasticity and shape-memory property of the hydrogel. a) Scheme and images showing the compression test process of a cylinder shaped hydrogel, the scale bar is 1 cm. b) The stress–strain curves of three repeated compression tests on the same hydrogel. c) Scheme illustration showing the process of heating, deforming, and recovering to test the shape-memory ability of the hydrogel. d) Photographs demonstrating the shape-memory ability of the hydrogels with different shapes, the scale bar is 1 cm. e) Shape recovery percentages of the gradient porous hydrogels, where W_o is the original hydrated mass of hydrogels and W_d is the rehydrated mass of the hydrogels after being subjected to the shape-memory process. f) Compressive stress–strain curves of original hydrogel (zero cycle) and hydrogels after being subjected to five cycles of the shape-memory process.

tuned by reversing their top surface. The results indicated that the directional bending of the hydrogel was due to the internal gradient porous structure instead of the laser irradiation direction. The nanoparticle loaded composite hydrogel was sliced into four pieces of hydrogel sheets with random thicknesses, and their laser-triggered bending behaviors were studied (Figure S22 and Video S3, Supporting Information). All of the hydrogel slices were observed to exhibit bending similar to that of the original integrated hydrogel.

The bending rates and bending angles of the gradient porous hydrogels in response to laser irradiation were investigated (Figure 4c–e). With increasing laser intensity, larger bending angles were obtained with a shorter irradiation time. The hydrogel exhibited rapid photoresponses, where a macroscale hydrogel strip with dimensions of 20 mm × 4 mm × 1 mm could bend from 0° to 70° in 5 s after 2.2 W cm^{-2} of laser irradiation (Figure 4d). In addition to rapid photoresponses, the hydrogel also exhibited a precise reversible bending motion in response to laser irradiation. Bending of the hydrogel can be fixed and maintained at a specific angle by maintaining a constant laser irradiation intensity. When the laser irradiation intensity was alternately increased and decreased, the hydrogels were reversibly bent or unbent back to their original angles (Figure 4e). The muscle-like bending ability of the gradient porous hydrogel was used to lift weights with different mass (Video S4, Supporting Information). A gradient porous hydrogel strip with dimensions of ≈15 mm × 4 mm × 1.5 mm could lift 700 mg of weights to a height of 10 mm under laser irradiation for 18 s (Figure 4f). As the mass of the weights was decreased, the value of the lifting height by the hydrogel increased (Figure S23, Supporting Information). The results suggested that the gradient porous elastic composite hydrogels have potential applications as a photomechanical converter for artificial muscles and soft robotics.

2.5. Laser-Driven Programmable Locomotion of Hydrogels

By modulating the laser positioning, the PPy nanoparticle loaded hydrogels could exhibit a variety of mechanical motions. As a demonstration, a PPy nanoparticle loaded gradient porous hydrogel strip was placed onto water and sequentially irradiated with NIR laser. The hydrogel strip could be bent or curved on both ends into a designated position, morphology, and direction

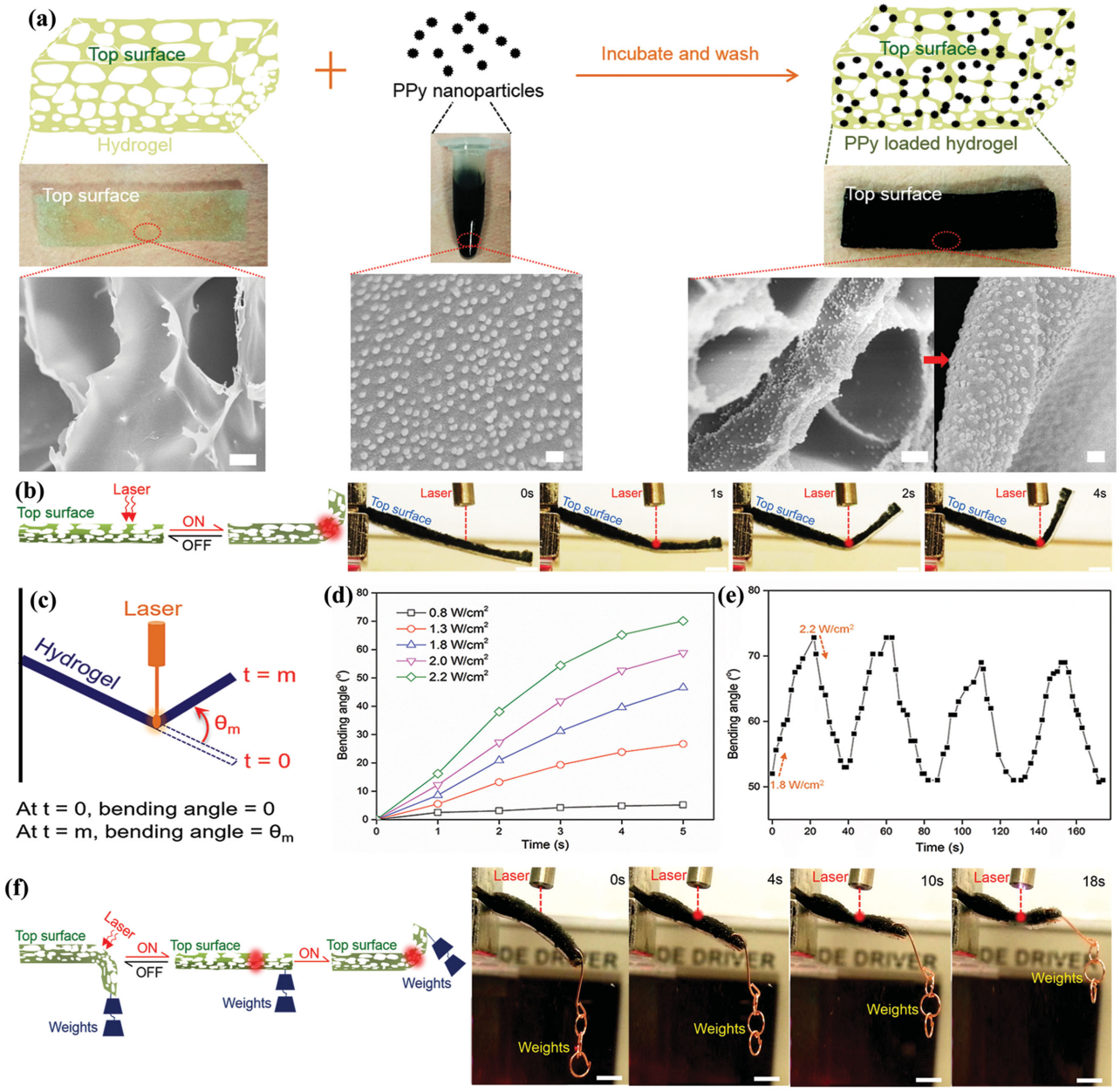

Figure 4. Photoresponse of PPy nanoparticles loaded hydrogel. a) The process of loading PPy nanoparticles into a gradient porous hydrogel and the corresponding SEM images for unloaded hydrogel (left, scale bar is 1 μm), PPy nanoparticles (middle, scale bar is 100 nm), and PPy nanoparticles loaded hydrogel (right, scale bar is 1 μm and 100 nm, respectively). b) Laser irradiation induced bending of a PPy nanoparticles loaded hydrogel strip, the scale bar is 1 mm. c) Scheme illustrating the definition and calculation of bending angles. d) Photo-responsive time and bending angles of the same hydrogel strip after being irradiated by laser with different intensity. e) The reversible bending and unbending of the hydrogel in response to alternate increase and decrease of laser irradiation intensity. f) The process of hydrogel to lift weights up with laser irradiation, the scale bar is 1 mm.

(**Figure 5**a–c). Moreover, we could even curl the whole hydrogel strip into a spiral pattern by moving the laser in a direction parallel to the hydrogel strip (Figure 5d and Video S5, Supporting Information). All these hydrogel motions were highly reversible and repeatable by simply switching the laser off and on for multiple cycles. Locomotion inspired by octopus-like swimming was imitated by controlling the laser to irradiate the middle part of a gradient porous hydrogel strip (Figure 5e and Video S6, Supporting Information). Because of the gradient porous structure of the hydrogel, the deswelling rate of the hydrogel top surface was greater than that of the hydrogel bottom surface (Figure S24a, Supporting Information). Consequently, the hydrogel strip bent in the direction of the top surface in a similar manner to the trailing arms of an octopus (Figure S24b, Supporting Information) when we used the laser to irradiate the middle of the hydrogel strip. The bending forces could be divided into the propulsive force and another force perpendicular to the hydrogel motion direction. Because of the rapid photoresponse and

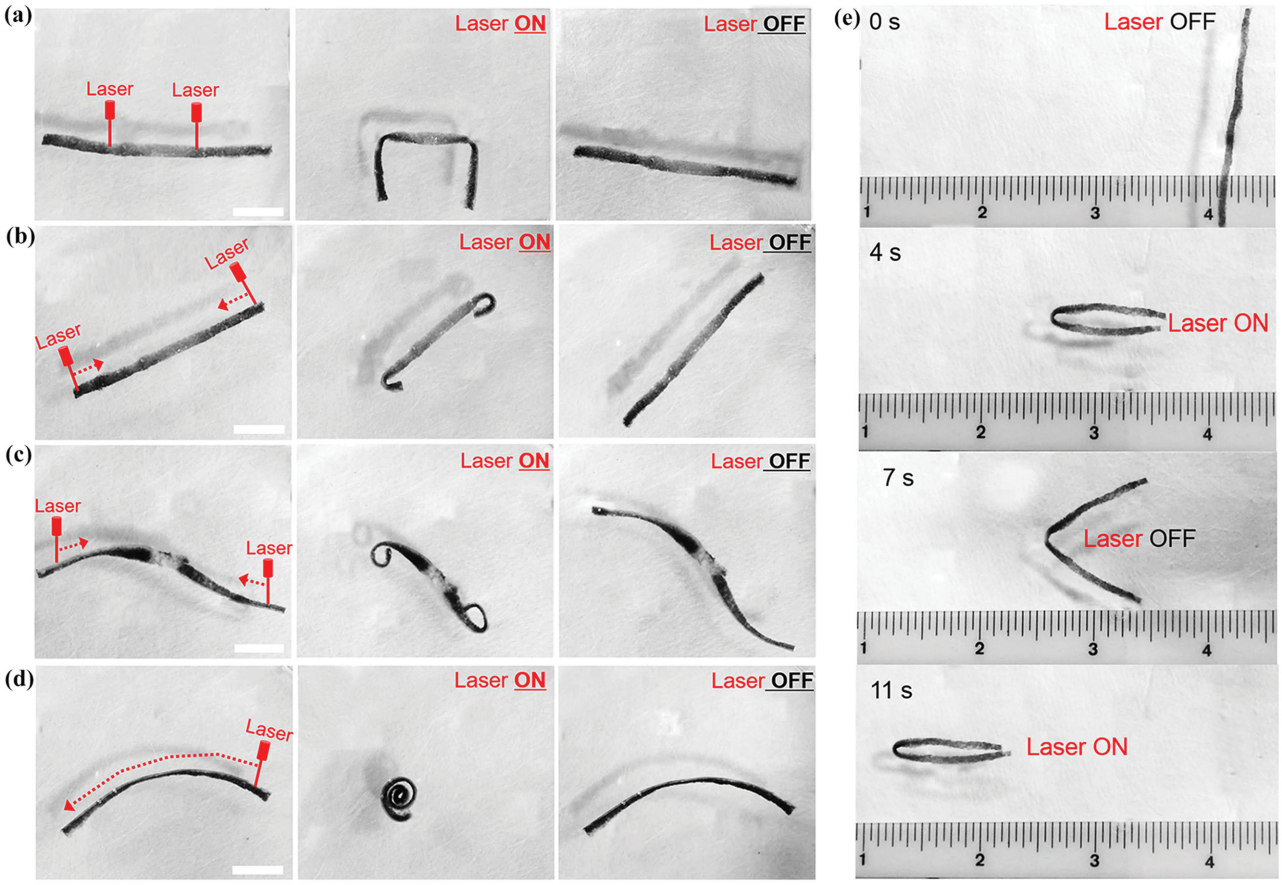

Figure 5. Laser irradiation to programmable locomotion of hydrogels. a,b) Folding and curving on both ends of the hydrogel strip to the same directions. c) Curving on both ends of a hydrogel strip to opposite directions. d) Curling the whole hydrogel strip into spiral pattern by moving the laser in a parallel direction along with the hydrogel, the scale bar is 1 cm. e) Optical image series showing the forward-moving hydrogel driven by laser irradiation.

elasticity of the hydrogel, the propulsive force was stronger than the drag force resulting from water resistance after laser irradiation, and thus the hydrogel strip was moved forward (Figure S24 and Video S6, Supporting Information). When the laser irradiation was stopped, the hydrogel strip swelled back to the original state because of the elasticity of the hydrogel, where the propulsive forces decreased rapidly with increasing drag force due to the increasing area of the hydrogel surface. Consequently, the hydrogel strip stopped moving. During the next laser irradiation, the movement of the hydrogel strip repeated the aforementioned processes, and the hydrogel moved past its original position.

3. Conclusion

In summary, we have presented a heterobifunctional crosslinker enabled hydrothermal process to synthesize gradient porous elastic hydrogels, thereby addressing the challenge of simultaneously improving response kinetics, mechanical properties, and anisotropic locomotion capability. The hydrogelation mechanisms outlined here are potentially applicable to numerous other composite systems consisting of thermal-responsive monomers and heterobifunctional crosslinkers, opening new avenues for modulating the pore structures of soft materials. Because of the excellent concurrent properties, the gradient porous elastic hydrogels can potentially provide superior performance to suit a variety of applications.

4. Experimental Section

Hydrothermal Synthesis of Gradient Porous Hydrogel: 500 mg of NIPAM (Sigma-Aldrich), 100 µL of 4HBA (Polysciences Asia Pacific, Inc.), and 5 mg of ammonium persulfate (APS, Sigma-Aldrich) were dissolved in 5 mL of DI H_2O, filtered and loaded into a 200 mL of hydrothermal reactor (Latech, Singapore). The reactor was subsequently heated in a 180 °C oven (Memmert, Germany) for 4 h. After the reactions, the hydrogels were peeled from the reactor, weighed and incubated in 1 L of DI H_2O for 2 d with regular changing of the H_2O. (This is the optimized hydrothermal reaction conditions. The optimizing process to obtain this reaction condition can refer to Sections S1 and S2, Supporting Information.)

Determination of Response Time of the Hydrogels: The response rate of the chemically crosslinked hydrogels was inversely proportional to the square of the hydrogel dimensions.[17] Consequently, hydrogels with specific dimensions were first prepared and then subjected to alternating thermal stimulation. The thermal response time was recorded until a complete shape change of the hydrogel was achieved. Briefly, a hydrogel strip with defined dimensions of 40 mm × 4 mm × 2.5 mm was first prepared and placed into a 25 °C water bath, where the end-to-end distance of the hydrogel strip was measured. Subsequently, the hydrogel strip was removed from the 25 °C water bath and immediately placed into a 40 °C water bath. The thermal response time was recorded according to the reduction of the

end-to-end distance of the hydrogel. Time recording was stopped until no further distance reduction of the hydrogel strip was observed. The heating/cooling processes were alternately repeated six times.

Compression Tests of Hydrogels: The hydrogels were punched into cylindrical-shaped specimens with a diameter and height of ≈8 mm and 2.5 mm, respectively. The compression tests were performed on a universal testing system (Instron) equipped with a 10 N force transducer. The hydrogel samples were compressed between two parallel plates in a uniaxial manner at a compression rate of 1.5 mm min^{-1}. The compressive modulus was determined on the basis of the slope of the initial linear region of the stress–strain curve. Three specimens were tested per experiment.

PPy Nanoparticles as Photothermal Transducer: PPy nanoparticles were prepared in aqueous solution containing poly(vinyl alcohol) (PVA) (M_w 9000–10 000, Sigma-Aldrich), $FeCl_3{\cdot}6H_2O$ (97%, Sigma-Aldrich), and pyrrole monomer (98%, Sigma-Aldrich). First, 0.75 g of PVA was dissolved in 10 mL of deionized water on a 60 °C hotplate for 20 min. After the solution was cooled down to room temperature, 0.63 g of $FeCl_3{\cdot}6H_2O$ was added to the PVA solution and stirred for 1 h. Subsequently, 69 µL of pyrrole monomer was added dropwise to the reaction mixture. The reaction mixture was maintained at 4 °C while being stirred for 24 h for the polymerization reaction. The resulting black PPy nanoparticle solution was centrifuged at 23 000 × g and 4 °C for 40 min to separate the PPy nanoparticles. The obtained PPy nanoparticles were then washed twice with deionized water. To investigate the ability of PPy nanoparticles to convert NIR light into heat, the PPy nanoparticle suspension was heated using NIR irradiation. 2 mL of PPy nanoparticles with different concentrations were placed into a 4 mL cuvette (1 cm path-length), which was put onto magnetic stirrer plate and kept stirring. The thermocouple of a digital thermometer with a precision of 0.1 °C (Fluke 51-II) was immersed into the solution. The PPy nanoparticle solution was then irradiated with a 980 nm laser for 10 min. The laser intensity was calculated using the equation, $(250/d^2) \times$ Output power, where d is the diameter of the laser beam in millimeter. Laser beam diameter was determined by using IR indication card. Output power is determined by power/energy meter Model 841-PE (Newport Opto-Electronics Technologies, Singapore) and the temperature changes were recorded every 10 s.

Loading PPy Nanoparticles into the Hydrogel: The hydrogels with specific dimensions (8 mm of diameter and 2.7 mm of height) were first hydrated and compressed to squeeze the excess water. Subsequently, 200 µL of PPy nanoparticles aqueous solution with a concentration of 4 mg mL^{-1} was added onto the hydrogels at room temperature. Due to the porous features of the hydrogels, PPy nanoparticles aqueous solution will be completely infiltrated into the hydrogels. The PPy nanoparticles loaded hydrogels were then incubated and washed thoroughly with water at room temperature for certain time (≈2 d) to remove the loosely bound PPy nanoparticles, during which the water was changed regularly and subjected to UV–vis analysis to monitor the PPy nanoparticles concentration changes. After the washing step, the PPy nanoparticles were tightly bound within the hydrogel matrix. The loading amount of PPy nanoparticles was obtained by equation $L = (A - W)\%$, where L is the final amount of PPy nanoparticles loaded within the hydrogel matrix, A is the actual amount of PPy nanoparticles added into the hydrogels, and W is the total amount of PPy nanoparticles being washed away during the washing step. To investigate if the PPy nanoparticles leak out from the hydrogel after temperature or laser stimulation, the PPy loaded hydrogels were incubated with 1 mL H_2O before the thermal or laser irradiation, the supernatant (pure H_2O) was analyzed with UV–vis–NIR spectrometer at 600–900 nm. After temperature stimulation on the hydrogels (40 °C for 10 min) or laser stimulation on the hydrogel (980 nm, 2.5 W cm^{-2} for 5 min), the supernatant was analyzed again with UV–vis–NIR spectrometer to see the changes of PPy nanoparticles absorbance values (Figures S17 and S18, Supporting Information, for more details).

Supporting Information

Supporting Information is available from the Wiley Online Library or from the author.

Acknowledgements

The authors thank the financial support from SMART innovation grant (R-397-000-146-592), Tier-1 grant (R-397-000-213-112), and NRF BDTA (R-397-000-221-592).

Received: August 15, 2015
Revised: September 19, 2015
Published online: October 26, 2015

[1] C. Weber, R. Hoogenboom, U. S. Schubert, *Prog. Polym. Sci.* **2012**, *37*, 686.
[2] Z. Hu, X. Zhang, Y. Li, *Science* **1995**, *269*, 525.
[3] D. Buenger, F. Topuz, J. Groll, *Prog. Polym. Sci.* **2012**, *37*, 1678.
[4] M. Nakahata, Y. Takashima, A. Hashidzume, A. Harada, *Angew. Chem. Int. Ed.* **2013**, *22*, 5731.
[5] D. J. Beebe, J. S. Moore, J. M. Bauer, Q. Yu, R. H. Liu, C. Devadoss, B. H. Jo, *Nature* **2000**, *404*, 588.
[6] E. Palleau, D. Morales, M. D. Dickey, O. D. Velev, *Nat. Commun.* **2013**, *4*, 2257.
[7] E. Wang, M. S. Desai, S. W. Lee, *Nano Lett.* **2013**, *13*, 2826.
[8] B. Yan, J. C. Boyer, D. Habault, N. R. Branda, Y. Zhao, *J. Am. Chem. Soc.* **2012**, *134*, 16558.
[9] J. Kim, M. J. Serpe, L. A. Lyon, *J. Am. Chem. Soc.* **2004**, *126*, 9512.
[10] S. Mura, J. Nicolas, P. Couvreur, *Nat. Mater.* **2013**, *12*, 991.
[11] S. R. Sershen, G. A. Mensing, M. Ng, N. J. Halas, D. J. Beebe, J. L. West, *Adv. Mater.* **2005**, *17*, 1366.
[12] C. W. Lo, D. Zhu, H. Jiang, *Soft Matter* **2011**, *7*, 5604.
[13] J. Yoon, P. Bian, J. Kim, T. J. McCarthy, R. C. Hayward, *Angew. Chem. Int. Ed.* **2012**, *51*, 7146.
[14] K. Haraguchi, H. J. Li, *Macromolecules* **2006**, *39*, 1898.
[15] E. S. Matsuo, T. Tanaka, *Nature* **1992**, *358*, 482.
[16] T. Fujigaya, T. Morimoto, Y. Niidome, N. Nakashima, *Adv. Mater.* **2008**, *20*, 3610.
[17] L. W. Xia, R. Xie, X. J. Ju, W. Wang, Q. Chen, L. Y. Chu, *Nat. Commun.* **2013**, *4*, 2226.
[18] A. Barbetta, G. Rizzitelli, R. Bedini, R. Pecci, M. Dentini, *Soft Matter* **2010**, *6*, 1785.
[19] N. Annabi, J. W. Nichol, X. Zhong, C. Ji, S. Koshy, A. Khademhosseini, F. Dehghani, *Tissue Eng. B* **2010**, *16*, 371.
[20] D. Wu, F. Xu, B. Sun, R. Fu, H. He, K. Matyjaszewski, *Chem. Rev.* **2012**, *112*, 3959.
[21] T. Asoh, M. Matsusaki, T. Kaneko, M. Akashi, *Adv. Mater.* **2008**, *20*, 2080.
[22] H. Therien-Aubin, Z. L. Wu, Z. Nie, E. Kumacheva, *J. Am. Chem. Soc.* **2013**, *135*, 4834.
[23] E. Zhang, T. Wang, W. Hong, W. Sun, X. Liu, Z. Tong, *J. Mater. Chem. A* **2014**, *2*, 15633.
[24] G. Stoychev, N. Puretskiy, L. Ionov, *Soft Matter* **2011**, *7*, 3277.
[25] A. Funke, F. Ziegler, *Biofuels, Bioprod. Biorefin.* **2010**, *4*, 160.
[26] R. Luo, C. H. Chen, *Chem. Commun.* **2015**, *51*, 6617.
[27] X. Sun, Y. Li, *Angew. Chem. Int. Ed.* **2004**, *43*, 597.
[28] A. B. Imran, K. Esaki, H. Gotoh, T. Seki, K. Ito, Y. Sakai, Y. Takeoka, *Nat. Commun.* **2014**, *5*, 5124.
[29] Y. Qiu, K. Park, *Adv. Drug Delivery Rev.* **2001**, *53*, 321.
[30] S. A. Bencherif, R. W. Sands, D. Bhatta, P. Arany, C. S. Verbeke, D. A. Edwards, D. J. Mooney, *Proc. Natl. Acad. Sci. USA* **2012**, *109*, 19590.
[31] A. Halperin, M. Kröger, *Langmuir* **2012**, *28*, 16623.
[32] S. A. Turner, J. Zhou, S. S. Sheiko, V. S. Ashby, *ACS Appl. Mater. Interfaces* **2014**, *6*, 8017.
[33] T. G. Leong, C. L. Randall, B. R. Benson, N. Bassik, G. M. Stern, D. H. Gracias, *Proc. Natl. Acad. Sci. USA* **2009**, *106*, 703.